Evaporation of liquid droplets on solid substrates. II. Periodic substrates with moving contact lines

Amirhossein Amini and G. M. Homsy*
Department of Mechanical Engineering, University of Washington, Seattle, Washington 98195, USA
(Received 10 June 2016; published 20 April 2017)

Experiments on evaporating droplets on structured surfaces have shown that the contact line does not move with constant speed, but rather in a steplike "stick-slip" fashion. As a first step in understanding such behavior, we study the evaporation of a two-dimensional volatile liquid droplet on a nonplanar heated solid substrate with a moving contact line and fixed contact angle. The model for the flat case is adapted to include curved substrates, numerical solutions are achieved for various periodic and quasiperiodic substrate profiles, and the dynamics of the contact line and the apparent contact angle are studied. In contrast with our results for a flat substrate, for which the contact line recedes in a nearly constant speed, we observe that the contact line speed and position show significant time variation and that the contact line moves in an approximate steplike fashion on relatively steep substrates. For the simplest case of a periodic substrate, we find that the apparent contact angle is periodic in time. For doubly periodic substrates, we find that the apparent contact angle is periodic and that the problem exhibits a phase-locking behavior. For multimode quasiperiodic substrates, we find the contact line behavior to be temporally complex and not only limited to a stick-slip motion. In all cases, we find that the overall evaporation is increased relative to the flat substrate.

DOI: 10.1103/PhysRevFluids.2.043604

I. INTRODUCTION

We consider the evaporation of a volatile liquid droplet on a nonplanar heated solid substrate for the case of a moving contact line and constant contact angle. A stick-slip motion of the contact lines, also referred to as steplike motion, has been reported in many experimental works [1,2] including the one by McHale *et al.* [3], in which they consider the evaporation of a small water droplet on structured polymer surfaces. As illustrated in their Fig. 2, they observe all three modes [4] of evaporation. (i) Initially the droplet evaporates in the pinned contact line mode. (ii) Once a critical contact angle is approached, the contact line is depinned and, in contrast with what occurs on a smooth surface, the contact line moves in a steplike fashion while the contact angle remains approximately constant. (iii) Finally, in the last and shortest stage of the evaporation, both the wetted radius and the contact angle decrease simultaneously until the entire droplet is evaporated. In this work we are interested in the middle stage in which the contact line shows a repetitive steplike behavior.

Most previous theoretical models [4,5] consider only mathematically smooth substrates. However, recent work has considered the dynamic contact line motion over a variety of nonplanar substrates driven by either capillary pressure or gravity. Savva and Kalliadasis [6] consider the spreading on horizontal nonplanar substrates of a two-dimensional droplet that has an initial shape different from the equilibrium profile. They consider different single-mode sinusoidal substrates, a trench, and a ridge, with the single-mode sinusoid being most relevant here. In similar work, Savva and Kalliadasis [7] consider gravity-driven motion of a drop on an inclined rough surface. The results in both of these papers demonstrate that in the case of a sinusoidal single-mode substrate, the contact line exhibits an apparent stick-slip behavior wherein it spends considerable time moving

*Corresponding author: bud@math.ubc.ca

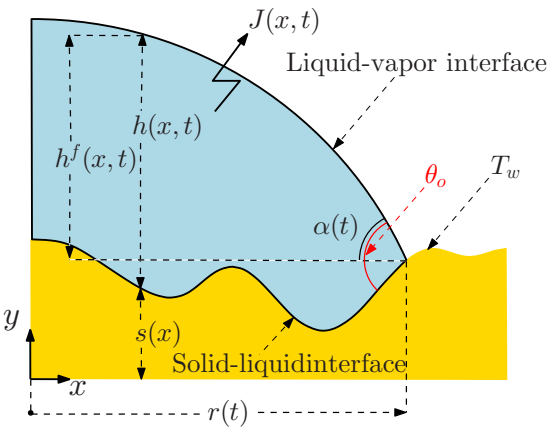

FIG. 1. Schematic of a droplet, evaporating on a symmetric nonplanar substrate, addressed in a Cartesian coordinate system.

very slowly, giving the appearance of being pinned. Savva *et al.* [8] generalized these observations by considering spreading over a random rough surface that is constructed from periodic waveforms with random Fourier coefficients. They find that the contact line response is also random and that spreading is inhibited by roughness. Espín and Kumar [9] provided a model of a spreading droplet on a single curved bump and commented on the potential for structured surfaces to produce apparent stick-slip behavior. By adopting the word "apparent" they emphasize that the pinning stage during the stick-slip motion needs to be interpreted as an apparent pinning since the contact line may still move very slowly. Here we will use the apparent stick-slip or apparent steplike terminology for the same reason described by these authors: The contact line may still move very slowly during the apparent pinning stage.

As far as we are aware, the problem of evaporating droplets on curved substrates is yet to be analyzed. Therefore, we have adapted our model in the preceding paper [10] to include surfaces with topography. Our model may be used to study curved substrate profiles for both modes of evaporation studied in the preceding paper: a pinned and a moving contact line with constant contact angle. However, since the results for the former were found to be very similar to the flat case, only the moving contact line case is considered here.

Accordingly, we include nonflat solid profiles in the evolution equation, boundary conditions, and numerical method provided in the preceding paper. We consider a single-mode harmonic solid as the simplest case of a periodic substrate and provide numerical solutions for the droplet shape and evaporative flux; we study the dynamics of the contact line and the apparent contact angle and show that an apparent stick-slip motion is captured by our model. We compare these results to the flat case and establish the characteristics of the contact line motion. We then create more complex substrate profiles by adding more modes, including quasiperiodic waveforms, and compare the results with the simpler cases.

II. PROBLEM DEFINITION

We consider a liquid layer evaporating on a symmetric nonplanar heated solid substrate and adopt the assumptions discussed in the preceding paper. As shown in Fig. 1, $h(x,t)$ denotes the local thickness of the liquid, $s(x)$ denotes the solid substrate profile, and $r(t)$ denotes the wetted radius. The contact angle, i.e., the angle between the solid and the interface at the contact line, is denoted by θ_0. The apparent contact angle, i.e., the angle that the liquid appears to make with the solid surface when viewed at such a coarse resolution that the substrate appears flat (the angle between the horizon and the interface at the contact line), is denoted by $\alpha(t)$. We represent the vertical distance between

the interface and the horizon at the contact line by an intermediate variable $h^f(x,t)$. Accordingly, $\alpha(t)$ and θ_0 are respectively defined by the slopes h_x^f and $h_x^f - s_x$ at $x = r(t)$. At any instance, $h^f(x,t)$ and the droplet thickness $h(x,t)$ are geometrically related as follows:

$$h(x,t) = h^f(x,t) + s(r(t)) - s(x). \tag{1}$$

The first derivative of (1) with respect to x at $r(t)$ implies that $\alpha(t)$ and θ_0 may be determined, respectively, by the slopes $h_x + s_x$ and h_x at the contact line. Hence, although defining h^f is essential to understand the geometry, the problem may be analyzed without its direct use.

The governing equations are modified for curved substrates and the problem is made dimensionless based on the same scaling as in the preceding paper. The equations are solved in the lubrication limit and as a result, the local evaporative mass flux remains

$$J = \frac{T_w - 1}{M + h(x,t)} \tag{2}$$

and the evolution equation [Eq. (7) of the preceding paper] becomes

$$h_t = -\frac{1}{3}\frac{\partial}{\partial x}((h+s)_{xxx}h^3) - \frac{T_w - 1}{M + h}. \tag{3}$$

The evaporative mass flux is identical to that for the flat case, but as a result of the normal stress balance $p - p_v = -(h+s)_{xx}$, the capillary flux term in the evolution equation is modified; for a comprehensive explanation of this see Ref. [11].

We take the initial condition that the liquid-vapor interface is part of a circle. Granted that $h^f(x,t)$ is symmetric and assuming that the first and third derivatives $s_x(0)$ and $s_{xxx}(0)$ of the solid-liquid profile at the location of symmetry line vanish, the symmetry boundary conditions remain

$$h_x(0,t) = 0, \quad h_{xxx}(0,t) = 0. \tag{4}$$

As in the preceding paper, at the contact line the droplet thickness is zero and the liquid pressure p is assumed to be in equilibrium with the vapor pressure p_v such that there is no pressure-driven flow into the contact line. These conditions, expressed for a curved substrate, are

$$h(r(t),t) = 0, \quad h_{xx}(r(t),t) + s_{xx}(r(t)) = 0. \tag{5}$$

The additional condition required to close this moving boundary problem is provided by assuming the contact angle to be constant during the evaporation, i.e.,

$$h_x(r(t),t) = \Theta_0. \tag{6}$$

Here Θ_0 is the scaled contact angle ($\Theta_0 = \theta_0/\epsilon$); for a comprehensive explanation of the scaled contact angle see Ref. [12]. As the contact line moves over the solid, $\alpha(t)$ adapts itself to the local slope $s_x(r(t))$ of the solid-liquid profile in such a way that the contact angle θ_0 remains fixed.

We are mainly interested in the effect of the solid-liquid profile on the droplet shape and contact line dynamics and less interested in their dependence on the dimensionless numbers T_w, M, and θ_0. Hence, we solve (3) for a variety of periodic and quasiperiodic substrates for fixed set of parameters: $T_w = 1.2$, $M = 2$, and $\theta_0 = 5^\circ$. However, in work not reported here, we observed qualitatively similar results for T_w in the range of 1.1–1.4, M in the range of 1–5, and $\theta(0)$ in the range of 5°–15°.

III. NUMERICS

Identical to the flat case, the method of lines is used to transform the partial differential equation into a system of ordinary differential equations and finite-difference schemes are employed to discretize the evolution equation at any given time level. However, due to the form of the capillary

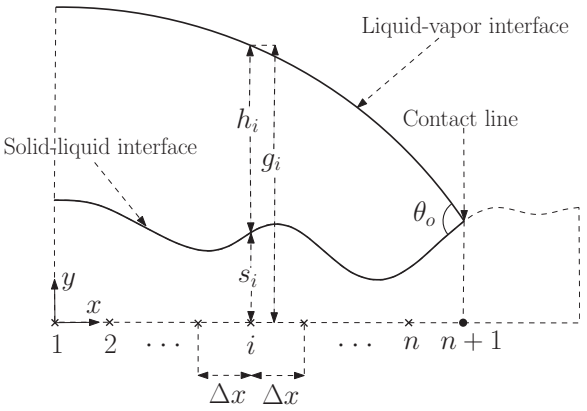

FIG. 2. Schematic of the computational domain at a given time step.

flux term, the discrete evolution equation is modified as

$$\frac{dh_i}{dt} = -\frac{1}{3\Delta x}\left(f_{i+1/2}\frac{g_{i+2} - 3g_{i+1} + 3g_i - g_{i-1}}{\Delta x^3} - f_{i-1/2}\frac{g_{i+1} - 3g_i + 3g_{i-1} - g_{i-2}}{\Delta x^3}\right) - \frac{T_w - 1}{M + h_i}. \tag{7}$$

As shown in Fig. 2, subscript i specifies the spatial node, Δx denotes the spatial mesh size, h_i and s_i denote the local thickness of the droplet and the solid profile, respectively, g_i denotes the liquid-vapor interface such that $g_i = h_i + s_i$, and $f_{i\pm1/2}$ represent averages of h_i^3 over adjacent nodes, i.e.,

$$f_{i\pm1/2} = \frac{h_i^3 + h_{i\pm1}^3}{2}. \tag{8}$$

The symmetry conditions (4) and the contact line conditions (5) and (6) are employed to evaluate (7) near the boundaries. To simultaneously evaluate the droplet shape and the position of the contact line, an operator splitting technique, similar to the flat case, is used. In the first stage, the evolution equation is solved over a time step assuming that the contact line is fixed. This produces an interface, shown in yellow in Fig. 3, which violates the constant contact angle condition (6). In the second stage, the contact line is moved a horizontal distance x^* such that at the new position the angle between the interface and the solid is equal to the prescribed contact angle θ_0. As discussed for the flat case, a Lagrange interpolating polynomial with three points is employed. However, since the contact angle is dependent on the slope s_x of the solid at the contact line and s_x varies with x, an iteration scheme is necessary to determine x^*. (This is in contrast to the flat case, in which the new position of the contact line is found analytically.) Once the contact line is moved, a new set of equally spaced spatial nodes is defined and the values of h are interpolated onto the new mesh.

The number of nodes at each time step and consequently the spatial mesh size Δx are chosen such that the distance x^* that the contact line moves is smaller than $\Delta x/2$. Also, an iterative method is employed to choose the size of the time step in the first stage such that all boundary conditions are satisfied to a specified accuracy at the end of the second stage. Once $h(x,t)$ and $r(t)$ are known, the evaporative mass flux $J(x,t)$ and the apparent contact angle $\alpha(t)$ are computed as secondary quantities.

The initial spatial mesh size is chosen to be on the order of 0.01 and the size of time step, which may change depending on the solid profile, is taken to be small enough such that with a 50% change in the spatial step size the solution changes no more than 0.1% and the contact angle equals the specified value with less than 5% error. We found a stiff solver to be necessary; hence, we use the MATLAB stiff solver `ode15s`.

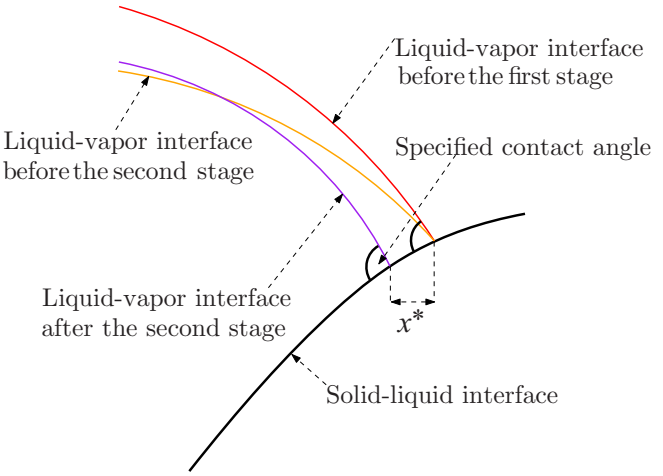

FIG. 3. Schematic of the liquid-vapor interface at different stages of the operator splitting method.

IV. SINGLE-MODE PERIODIC SUBSTRATES

Consider the single-mode periodic substrate of wavelength λ shown in Fig. 4. Since the first and third derivatives of the solid-liquid interface vanish at the center, the droplet symmetry line must meet the solid-liquid interface at either a peak or a trough. Since we do not expect fundamentally different behaviors between these cases, only the latter configuration is considered in this work. Accordingly, the height $s(x)$ of the solid-liquid interface is described by

$$s(x) = -a\cos(kx), \tag{9}$$

where a is the amplitude and k is the wave number, i.e., $k = 2\pi/\lambda$.

As a result of choosing $h^f(0,0)$ and $r(0)$ as the length scales in x and y directions, the solid-liquid interface in dimensionless form is

$$s(x) = -A\cos(\Gamma x), \tag{10}$$

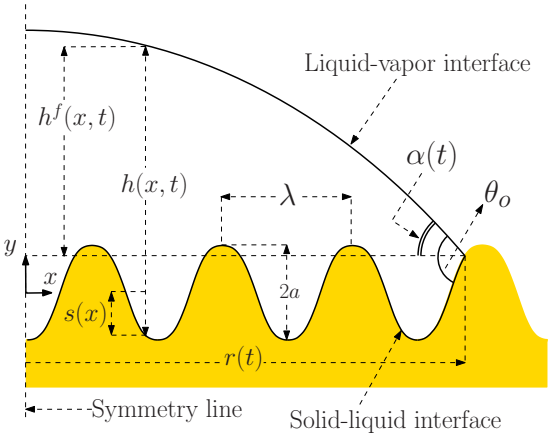

FIG. 4. Schematic of a 2D drop on a periodic solid substrate.

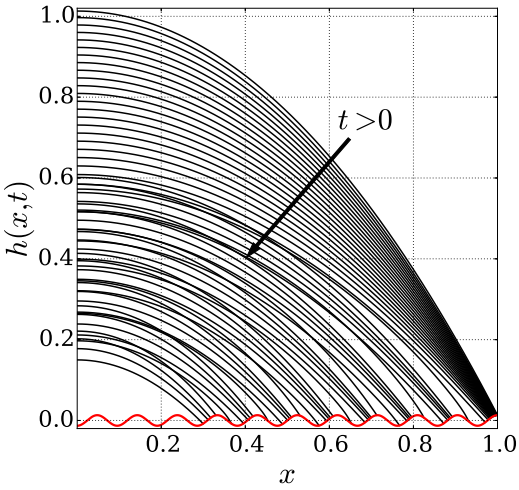

FIG. 5. Droplet profile while evaporating on the single-mode periodic solid substrate, for the reference case. (Profiles are plotted over equal time increments.)

where A is the scaled amplitude

$$A = \frac{a}{h^f(0,0)} \tag{11}$$

and Γ is the dimensionless wave number

$$\Gamma = r(0)k. \tag{12}$$

Accordingly, $\Gamma/2\pi$ is the number of wavelengths (on each side of the symmetry line) that are covered initially by the droplet. To apply the lubrication approximation, the droplet aspect ratio $\epsilon = L_y/L_x$, determined by the specified contact angle θ_0, must obey $\epsilon \ll 1$. Additionally, to ensure that the substrate profile also follows the lubrication approximation, the dimensionless slope ξ, defined as

$$\xi = ak, \tag{13}$$

must obey $\xi \ll 1$. The three dimensionless numbers A, Γ, and ξ are not independent, i.e.,

$$\xi = \epsilon A \Gamma, \tag{14}$$

hence assigning values to any two of them is sufficient to describe the substrate.

As a reference case, we take a droplet that initially covers 10.5 wavelengths of the solid on each side of the symmetry line (i.e., $\Gamma/2\pi = 10.5$), a prescribed contact angle $\theta_0 = 5^\circ$, and a solid slope ratio $\xi = 2\pi \times 0.006$. Such a configuration has $\epsilon = 0.0437$ and $A = 0.0131$. Additionally, numerical solutions were obtained for $\Gamma/2\pi$ in the range of 6–15.5 and $\xi/2\pi$ in the range of 0.003–0.006, but will not be presented since they are qualitatively similar to those for the reference case.

Figure 5 illustrates the droplet shape evolution for the reference case. As anticipated, the droplet thickness decreases on average; however, due to the global effect of the contact line motion over peaks and troughs, h shows nonmonotonic variation near the centerline. Since the droplet adapts its shape to the local slope of the solid such that the contact angle remains fixed, the droplet profile varies from its initial shape and thus simpler models, which *assume* that the droplet cross section remains circular along the evaporation, are not valid. For the reference case presented, the mean square error of the departure of the profile from a static shape is on the order of 5%.

Results for $J(x,t)$ are presented in Fig. 6. Consistent with Eq. (2), the evaporative flux increases similarly to the flat case: Its maximum is located at the contact line and the maximum value is constant over time. However, on a periodic substrate, (i) J is oscillatory along the x axis since the

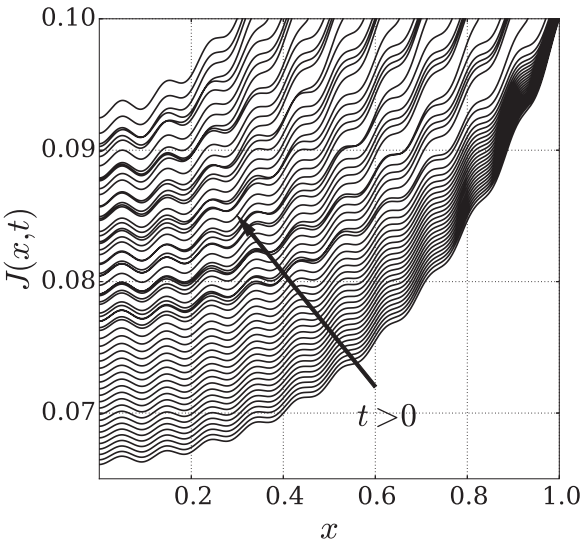

FIG. 6. Evaporative mass flux of an evaporating droplet on the single-mode periodic solid substrate, for the reference case.

substrate is sinusoidal and (ii) some minor temporal variation is observed near the centerline as a consequence of the discussed temporal variation in h.

The wetted radius $r(t)$ is plotted for both the reference case and the corresponding flat substrate in Fig. 7. In contrast to what we found for the flat case, $r(t)$ exhibits a periodic time variation superposed on a linear decrease, indicating that the speed u_{cl} of the contact line in the x direction is no longer constant. Figure 7 also shows that the slope of a linear fit to $r(t)$ (neglecting the initial transient), i.e., the average velocity $\bar{u}$ of the contact line, is approximately 25% larger than the constant contact line speed u_f observed for the flat case. Interestingly, for all the cases we studied, we found that $\bar{u}$ is larger than u_f and that while it is only weakly dependent on Γ, it increases with increasing slope

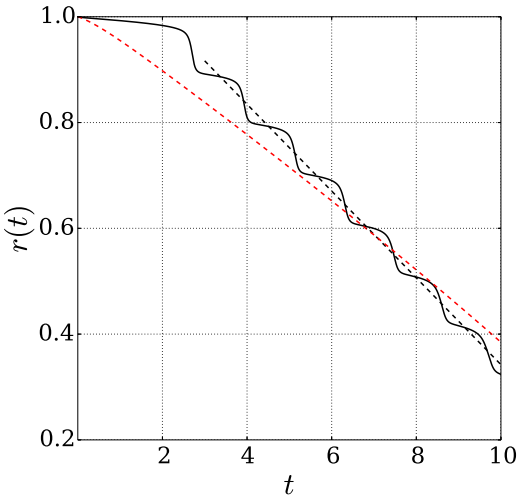

FIG. 7. Wetted radius $r(t)$ on the single-mode periodic solid substrate, for the reference case. The black dashed line represents the fitted line to $r(t)$, neglecting the initial transient, and the red dashed line represents the results for the flat case. The slopes of the black and red dashed lines are 0.081 and 0.065, respectively.

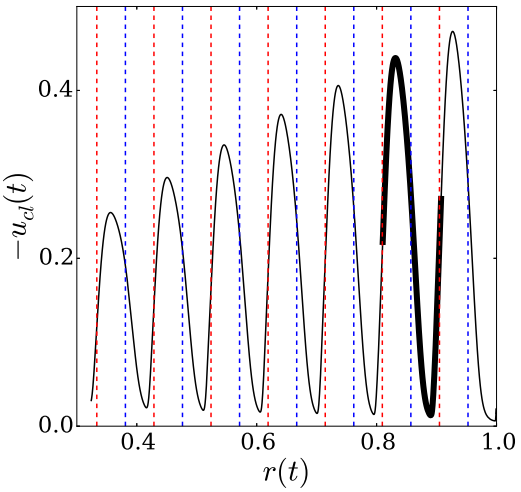

FIG. 8. Contact line speed u_{cl} as a function of the wetted radius $r(t)$, for the reference case. The red and blue dashed lines represent the location of peaks and troughs, respectively. The thick region corresponds to the motion over the second period of the solid.

ratio ξ. The fact that $\bar{u} \neq u_f$ is consistent with the nonlinearity of the problem, but to investigate why nonlinearities lead to faster average evaporation, further analysis is required regarding the contact line motion.

To relate the dynamics of the contact line to the solid profile, the (negative) values of u_{cl} are plotted as a function of $r(t)$ and presented in Fig. 8. The red and blue dashed lines represent the location of peaks and troughs respectively, so that at any instant, one can identify the contact line speed and position, simultaneously. Focusing on one cycle (shown as a black solid curve in Fig. 8), the contact line slows from the peak to the first inflection point; it accelerates between the first and second inflection points such that its maximum is achieved near the second, after which it slows down until it reaches the second peak. The contact line dynamics during the subsequent periods is similar, except that both the maximum speed of contact line and the speed at which it moves over the peaks decrease. To analyze this behavior, each term on the right-hand side of the evolution equation (3) was evaluated and monitored separately over time. The results indicate that the capillary flux term dominates the evaporative flux near the contact line and therefore the motion is governed mainly by the shape of the solid. At any time, the distance required for the contact line to move such that the specified contact angle is maintained, and consequently the instantaneous speed of the contact line, is highly dependent on the substrate profile. As shown in Fig. 8, the contact line loses speed where the solid curvature is negative and gains speed otherwise.

Rather than plotting the contact line speed as a function of location (Fig. 8), it is plotted as a function of time in Fig. 9. As can be seen, for each period of the solid, the motion may be divided into a low-speed phase, in which $u_{cl} < u_f$, and a high-speed phase, which includes a spike. The dashed box, which zooms in on one of these low-speed and high-speed regions, indicates that (i) during a low-speed period the speed is near zero and (ii) the duration of a low-speed region is relatively long. Accordingly, one who monitors the location of the contact line with limited accuracy might assume that it is pinned for a range of time mimicking a steplike motion. Thus, a steplike motion is captured by our lubrication model. This steplike motion is qualitatively similar to the experimentally observed stick-slip behavior of the contact line and is consistent with the apparent stick-slip behavior described by Espín and Kumar [9] and Savva and Kalliadasis [6], discussed in the Introduction.

The apparent contact angle $\alpha(t)$ is plotted as a function time in Fig. 10(a). Recall that $\alpha(t)$ adjusts its value to the local slope of the solid $s_x(r(t))$ such that the contact angle remains constant. As a result, the points at which $\alpha = \theta_0$ correspond to peaks (shown with cyan circles) and troughs and

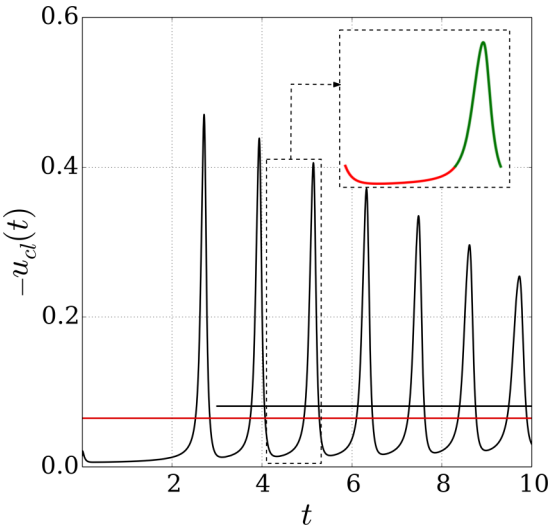

FIG. 9. Contact line speed $u_{cl}(t)$ on the periodic solid substrate, for the reference case. The dashed box represents the results for one low-speed region shown in red followed by a high-speed spike illustrated in green. The black horizontal line represent the average speed $\bar{u}$, neglecting the initial transition. The red line denotes u_f, the speed for the flat case. For the data presented, $\bar{u}$ and u_f are equal to 0.081 and 0.065, respectively.

the points at which α reaches its maximum or minimum values correspond to the inflection points of the solid profile. Except for an initial transient, the distance between two adjacent cyan circles is constant over the entire process, meaning that the time t_λ that it takes for the contact line to move from one peak to another is constant, i.e., $\alpha(t)$ is a periodic function. Although this may be discovered from plots like those in Figs. 7 and 9, focusing on $\alpha(t)$ allows a convenient analysis of the dynamics by Fourier decomposition.

Figure 10(b) shows the power spectrum of $\alpha(t)$ in blue. We see that all the major peaks are located at the frequencies that are harmonics of a single primary frequency $f_p = 1/t_\lambda$. As mentioned earlier,

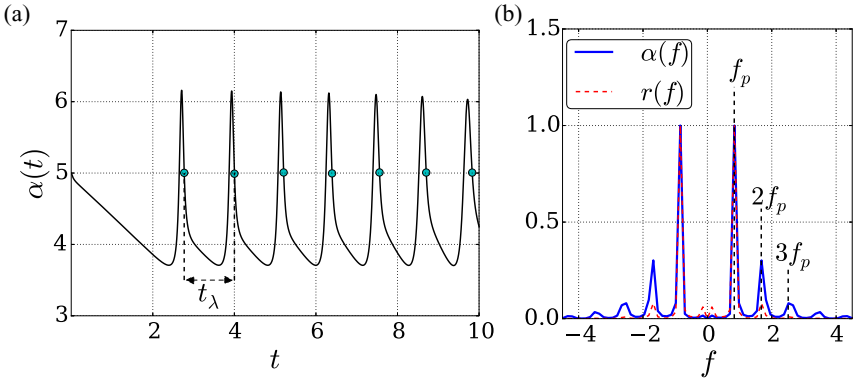

FIG. 10. Apparent contact angle α on a single-mode periodic substrate, for the reference case. (a) α as a function of time. The cyan circles represent the time at which the contact line is located on a peak; the distance between each pair of adjacent circles denotes the time t_λ that it takes for the contact line to move over one wavelength of the solid. (b) Normalized power spectrum of $\alpha(t)$ (shown in blue) and $r(t)$ (shown in red), neglecting the initial transient. All the major peaks are located at harmonics of $f_p = 0.84$, indicating that $t_\lambda = 1.19$.

the contribution of these harmonics to the mean speed is such that the nonlinearity of the solid leads to faster evaporation. As expected, we found that once the linear signal is subtracted from $r(t)$, the peaks in the power spectrum of the resulting values are also located exactly at harmonics of $f_p = 1/t_\lambda$. This is illustrated with red dashed lines in Fig. 10(b).

We generated similar results for different values of ξ and Γ and found that while f_p increases with increasing ξ and Γ, the behavior of the contact line is qualitatively similar for all cases. Therefore, we conclude that for any given single-mode periodic substrate, the time t_λ that it takes for the contact line to travel one wavelength is independent of how far the corresponding wavelength is from the centerline, i.e., $\alpha(t)$ is a periodic function. Such a conclusion may be validated by showing that the total average speed $\bar{u}$ is equal to the average speed for each wavelength λ/t_λ. This equality is found to be satisfied for all cases we studied, including the case presented for which $\bar{u} = 0.081$ and $\lambda/t_\lambda = 0.08$.

In summary, for contact line motion on a single-mode periodic substrate, we found that (i) the apparent stick-slip behavior is captured by our lubrication model; (ii) the nonlinearity of the problem leads to faster evaporation such that the average speed $\bar{u}$ of the contact line is larger than the constant speed u_f observed for the flat case; (iii) the apparent contact angle $\alpha(t)$ is periodic, i.e., the average speed λ/t_λ for each period is constant over different wavelengths and therefore is the same as the global average speed $\bar{u}$; and (iv) as expected of a nonlinear system with periodic coefficients, the power spectrum of α shows a typical single-mode with harmonics behavior.

V. TWO-MODE PERIODIC SUBSTRATES

Having established what happens in the simplest case of a periodic substrate, the question is what happens with a more complex substrate variation. One way to approach this question is to build up complexity by adding more modes.

We generated a two-mode periodic substrate $s_2(x)$ by a linear combination of a high-frequency $s_H(x)$ and a low-frequency $s_L(x)$ harmonic function, i.e.,

$$s_2(x) = -\frac{1}{2}\left[\overbrace{a_H \cos(k_H x + \phi_H)}^{-s_H(x)} + \overbrace{a_L \cos(k_L x + \phi_L)}^{-s_L(x)}\right]. \tag{15}$$

To ensure that the droplet center is over a trough we choose $\phi_H = \phi_L = 0$, for simplicity we take $a_H = a_L = a$, and to scale the problem in x and y directions we choose $r(0)$ and $h^f(0,0)$. As a result, the dimensionless form of $s_2(x)$ is

$$s_2(x) = -\sum_{i=1}^{2} \frac{A}{2} \cos(\Gamma \Omega_i x), \tag{16}$$

where

$$A = \frac{a}{h^f(0,0)}, \quad \Gamma = r(0)k_L, \quad \Omega_1 = \frac{k_H}{k_L}, \quad \Omega_2 = 1. \tag{17}$$

The slope of such a substrate is bounded by a dimensionless number ξ_2, defined as

$$\xi_2 = a(k_H + k_L), \tag{18}$$

and hence $\xi_2 \ll 1$ serves as a sufficient condition for the lubrication approximation to be valid. This slope ratio is dependent on the the other dimensionless numbers via

$$\xi_2 = \epsilon A \Gamma \sum_{i=1}^{2} \Omega_i. \tag{19}$$

Thus, assigning values to Ω_1, A, and Γ and choosing a contact angle θ_0 is sufficient to describe the problem.

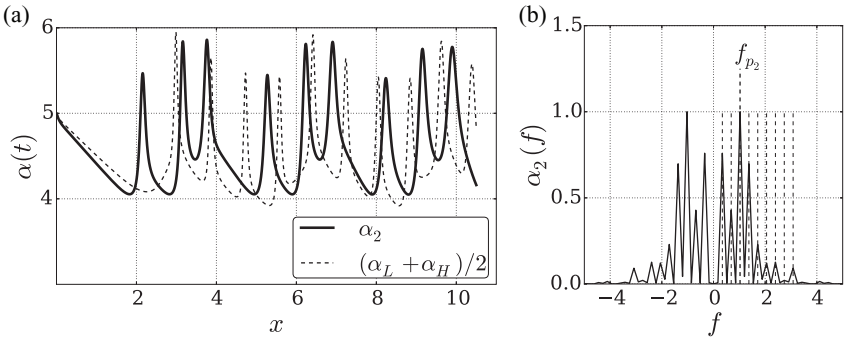

FIG. 11. Apparent contact angle as the droplet evaporates on the two-mode periodic solid substrate, for the reference case. (a) α_2 as a function of time. The dashed line represents the average of α_L and α_H, which are the contact angles produced as a result of separately solving the problem on s_L and s_H, respectively. (b) Normalized power spectrum of $\alpha_2(t)$, neglecting the initial transient. All the major peaks are located at either harmonics or subharmonics of f_p. The primary frequencies for this case are $f_{p_2} = 1.0272$, $f_{p_H} = 1.207$, and $f_{p_L} = 0.229$.

As a reference case, a two-mode substrate s_2 with $\Omega_1 = 3$, $A = 0.0076$, and $\Gamma/2\pi = 4.5$ and a droplet with contact angle $\theta_0 = 5^\circ$ were considered. In order to probe nonlinearities and to test for superposition, the problem is solved for s_2, s_L, and s_H, separately. For each substrate, the numerical solution is achieved over 10.5 units of dimensionless time, which is enough for the contact line to move over three wavelengths on s_2 and s_L and nine wavelengths on s_H.

The black line in Fig. 11(a) gives the apparent contact angle $\alpha_2(t)$ for evaporation on s_2. As shown, $\alpha_2(t)$ is a more complex waveform compared to the single-mode case but is still periodic. One may interpret $\alpha_2(t)$ as a periodic waveform with fundamental frequency f_{p_2} that is modulated by a subharmonic carrier signal of frequency $f_{p_2}/3$. Figure 11(b) quantitatively confirms such an interpretation by showing that all the peaks of the power spectrum are located at frequencies that are either subharmonics or superharmonics of a single primary frequency f_{p_2}. As a result, the time t_{λ_2} that it takes for the contact line to move over one wavelength of s_2 is constant during the evaporation. Accordingly, similar to what we found for the single-mode substrate, the average speed λ_2/t_{λ_2} of each period is the same for all wavelengths of s_2 and is equal to the global average speed $\bar{u}_2$. (Note that $\lambda_2 = 2\pi/\Gamma$ and for this case $t_{\lambda_2} = 3/f_{p_2}$.)

We found that a linear superposition of the results for single modes fails to predict the solution on s_2; this is expected since the problem is nonlinear. Figure 11(a) confirms this by showing the disparity between the average solution $(\alpha_L + \alpha_H)/2$ and the two-mode solution α_2. Additionally, we investigated the dependence of the primary frequency f_{p_2} of the two-mode substrate on the single-mode frequencies f_{p_H} and f_{p_L} and thus calculated each separately. Interestingly, we found that regular sums and differences of f_{p_H} and f_{p_L} or simple relations involving Ω_1 fail to predict f_{p_2} and thus we conclude that the problem exhibits a phase-locking behavior for this case.

The (negative) values of the contact line speed u_{cl_2} are presented in Fig. 12. As can be seen, the results are more complex than those for the single-mode substrates, but follow the same overall apparent stick-slip behavior: The maxima decrease while the width of the high-speed regions increases such that the global average speed $\bar{u}_2$ is the same as the average speed $\lambda_2 f_{p_2}/3$ for each period. This is verified for the reference case since the average speed $\bar{u}_2$, shown with the horizontal line in Fig. 12, is in good agreement with $\lambda_2 f_{p_2}/3$.

We generated many two-mode periodic substrates with different rational values of Ω_1 and solved the problem separately for the two-mode substrate and each of its corresponding single-mode profiles. We found that (i) similar to the single-mode profiles, the contact line exhibits an apparent stick-slip behavior; (ii) the apparent contact angle is still periodic but the peaks of its power spectrum are located at the subharmonics and harmonics of a single primary frequency f_{p_2}; (iii) the overall evaporation is faster compared to the flat case; (iv) due to the strong nonlinearity of the problem, the

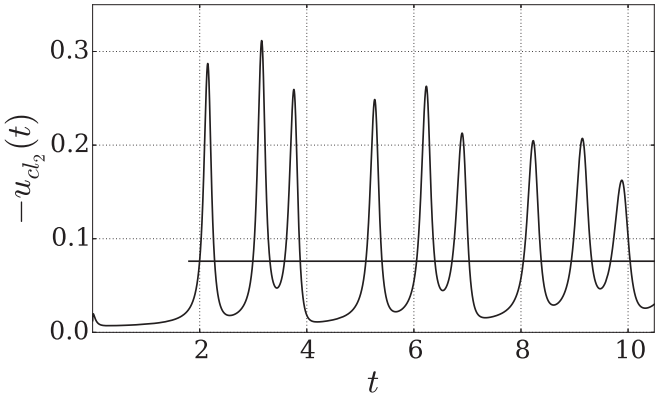

FIG. 12. Contact line speed $u_{cl_2}(t)$ as the droplet evaporates on the two-mode periodic solid substrate, for the reference case. The horizontal line represents the global average speed $\bar{u}_2$, neglecting the initial transient. For the data presented, $\bar{u}_2 = 0.0760$.

solution for two-mode substrates may not be obtained by the linear superposition of the single-mode results; and (v) sums and differences of single-mode frequencies f_{p_L} and f_{p_H} fail to produce the primary frequency f_{p_2} of the two-mode case and there is no simple relation between f_{p_2}, f_{p_L}, and f_{p_H} that holds for all values of Ω_1. We conclude that the interesting phase-locking behavior is a general result over the range of parameters studied.

VI. MULTIMODE QUASIPERIODIC SUBSTRATES

Our model is not limited to the periodic substrates and is therefore capable of solving the problem for any 2D symmetric solid profile. Hence we studied shapes that are closer to a random configuration. The number of modes was increased to add complexity and irrational values were assigned to the wavelength ratios Ω_i to create quasiperiodic shapes. Here we consider the reference case in which three modes are combined as

$$s_3(x) = -\sum_{i=1}^{3} \frac{A}{3} \cos(\Gamma \Omega_i x), \tag{20}$$

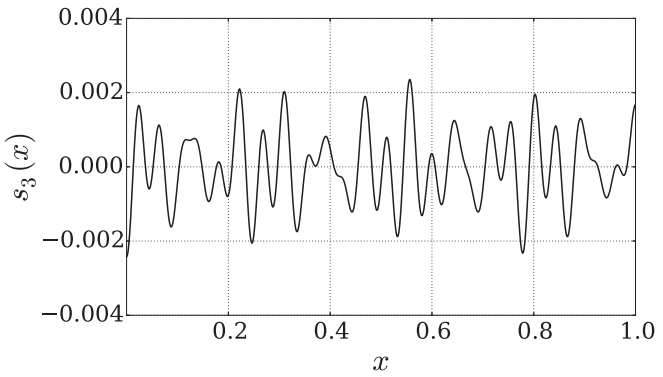

FIG. 13. Three-mode substrate produced by irrational wavelength ratios $\Omega_1 = 2\pi/3$, $\Omega_2 = \sqrt{\pi}$, and $\Omega_3 = 1$.

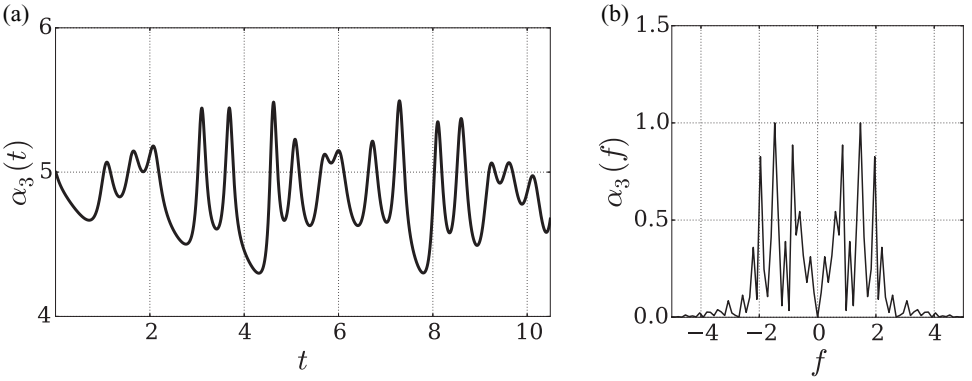

FIG. 14. Results for three-mode substrate produced by irrational wavelength ratios $\Omega_1 = 2\pi/3$, $\Omega_2 = \sqrt{\pi}$, and $\Omega_3 = 1$ and the specified contact angle $\theta_0 = 5^\circ$. (a) Apparent contact angle α_3 over time. (b) Normalized power spectrum of $\alpha_3(t)$, neglecting the initial transient. In contrast with periodic substrates, the peaks are not located at harmonics (or subharmonics) of a single primary frequency.

with the wavelength ratios chosen as

$$\Omega_1 = \frac{2\pi}{3}, \quad \Omega_2 = \sqrt{\pi}, \quad \Omega_3 = 1, \tag{21}$$

$\Gamma/2\pi \approx 1.85$ and $A = 0.0024$. Figure 13 shows the corresponding quasiperiodic solid-liquid interface, which is no longer periodic and appears fairly random.

The problem is solved numerically with contact angle $\theta_0 = 5^\circ$. The apparent contact angle $\alpha_3(t)$ and its power spectrum $\alpha_3(f)$ are shown in Figs. 14(a) and 14(b), respectively. In contrast to single-mode and two-mode periodic solids, (i) the apparent contact angle exhibits a complex nonperiodic waveform and (ii) the peaks of its power spectrum are no longer located at harmonics or subharmonics of a single primary frequency.

The contact line speed u_{cl_3} is plotted as a function of time in Fig. 15. Similar to the periodic substrates, as the contact line recedes towards the centerline an overall decrease is observed in the local maxima of u_{cl_3} and the total evaporation is faster compared to the flat case (for the reference case presented, the average velocity of the contact line is approximately 5% larger than the constant contact line speed observed for the flat case). However, for this three-mode quasiperiodic substrate, the contact line exhibits a more complex and random behavior. Although the apparent stick-slip

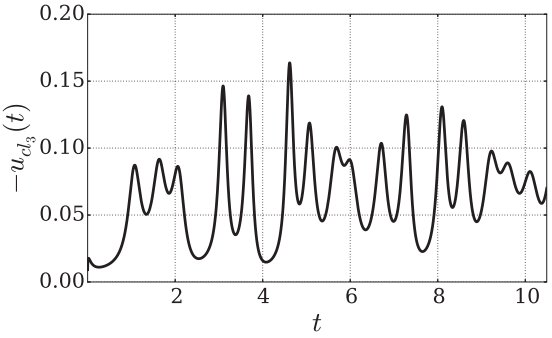

FIG. 15. Contact line speed $u_{cl_3}(t)$ for the three-mode substrate produced by irrational wavelength ratios $\Omega_1 = 2\pi/3$, $\Omega_2 = \sqrt{\pi}$, and $\Omega_3 = 1$ and the specified contact angle $\theta_0 = 5^\circ$. Neglecting the initial transient, the global average speed $\bar{u}_3$ for the data presented is equal to 0.068.

motion is observed in some regions, the dynamics are much more complicated and hence it may not be interpreted as a pure steplike motion. It is to be expected that as the substrate becomes more complicated, the spectrum will become broadened and the contact line speed will approximate a stationary random function.

VII. SUMMARY

The evaporation of a 2D symmetric sessile drop on heated nonplanar solid substrates was studied for the case in which the contact line is moving and the contact angle is fixed. The evolution equation, boundary conditions, and numerical method provided for the flat solid in the preceding paper were modified accordingly. The parameters T_w, M, and θ_0 were chosen to be fixed and the problem was solved for a variety of periodic and quasiperiodic substrates. Qualitatively similar behaviors were observed over a range of values of the parameters, but were not presented here in the interest of brevity.

In contrast with what we found for the flat substrate, our results for the single-mode periodic profiles indicate that the droplet cross section varies from the initial circular shape and the wetted radius $r(t)$ is a nonlinear oscillatory function of time. We found that the overall evaporation is faster compared to the flat substrates and as the contact line recedes towards the centerline, it exhibits an apparent stick-slip behavior including two phases: a relatively long apparent-pinning stage, in which the contact line moves slowly, followed by a shorter high-speed region in which the speed of the contact line shows a spike. Moreover, the apparent contact angle $\alpha(t)$ was found to be periodic, meaning that the time t_λ that it takes for the contact line to move over one wavelength is constant. As the maximum speed of the contact line decreases, the duration of the high-speed regions increases in such a way that t_λ remains constant over the entire process. Finally, as expected from a nonlinear system with periodic coefficients, we found that all the peaks in the power spectrum of $\alpha(t)$ are located at the harmonics of a single primary frequency f_p.

For the two-mode periodic solid profiles, our results show the same apparent stick-slip behavior, the apparent contact angle is still periodic, all the peaks of the power spectrum of α are located at the harmonics and subharmonics of a single primary frequency f_{p_2}, and the overall evaporation is faster compared to the flat case. However, compared to the single-mode solid, the apparent contact angle is a more complex waveform and more harmonics and subharmonics are observed in its power spectrum. Additionally, we found that the nonlinearity is strong enough such that the solution of the two-mode profile may not be achieved from the single-mode results. In other words, the problem behaves as a phase-locking system and thus combining the corresponding single-mode frequencies in sums and differences fails to predict the primary frequency f_{p_2}.

Finally, for a multimode quasiperiodic profile that resembles a random configuration, we found that while the evaporation is still faster compared to the flat case, the contact line behavior is very complex and not limited to an apparent stick-slip motion. We also found that the apparent contact angle is no longer periodic and the peaks in the power spectrum of the apparent contact angle are associated with different primary frequencies, i.e., the peaks are no longer located at the harmonics or subharmonics of a single primary frequency.

[1] D. Orejon, K. Sefiane, and M. E. Shanahan, Stick-slip of evaporating droplets: Substrate hydrophobicity and nanoparticle concentration, Langmuir **27**, 12834 (2011).

[2] N. Anantharaju, M. Panchagnula, and S. Neti, Evaporating drops on patterned surfaces: Transition from pinned to moving triple line, J. Colloid Interface Sci. **337**, 176 (2009).

[3] G. McHale, S. Aqil, N. J. Shirtcliffe, M. I. Newton, and H. Y. Erbil, Analysis of droplet evaporation on a superhydrophobic surface, Langmuir **21**, 11053 (2005).

[4] J. M. Stauber, S. K. Wilson, B. R. Duffy, and K. Sefiane, On the lifetimes of evaporating droplets, J. Fluid Mech. **744**, R2 (2014).

[5] N. Murisic and L. Kondic, On evaporation of sessile drops with moving contact lines, J. Fluid Mech. **679**, 219 (2011).
[6] N. Savva and S. Kalliadasis, Two-dimensional droplet spreading over topographical substrates, Phys. Fluids **21**, 092102 (2009).
[7] N. Savva and S. Kalliadasis, Droplet motion on inclined heterogeneous substrates, J. Fluid Mech. **725**, 462 (2013).
[8] N. Savva, S. Kalliadasis, and G. A. Pavliotis, Two-Dimensional Droplet Spreading Over Random Topographical Substrates, Phys. Rev. Lett. **104**, 084501 (2010).
[9] L. Espín and S. Kumar, Droplet spreading and absorption on rough, permeable substrates, J. Fluid Mech. **784**, 465 (2015).
[10] A. Amini and G. M. Homsy, Evaporation of liquid droplets on solid substrates. I. Flat substrate with pinned or moving contact line, preceding paper, Phys. Rev. Fluids **2**, 043603 (2017).
[11] L. E. Stillwagon and R. G. Larson, Fundamentals of topographic substrate leveling, J. Appl. Phys. **63**, 5251 (1988).
[12] D. T. Moyle, M. S. Chen, and G. M. Homsy, Nonlinear rivulet dynamics during unstable wetting flows, Int. J. Multiphase Flow **25**, 1243 (1999).